GEOPHYSICS, VOL. 65, NO. 6 (NOVEMBER-DECEMBER 2000); P. 1818–1830, 6 FIGS., 1 TABLE.

Estimation of fracture parameters from reflection seismic data—Part III: Fractured models with monoclinic symmetry

Andrey Bakulin*, Vladimir Grechka‡, and Ilya Tsvankin‡

ABSTRACT

Geophysical and geological data acquired over naturally fractured reservoirs often reveal the presence of multiple vertical fracture sets. Here, we discuss modeling and inversion of the effective anisotropic parameters of two types of fractured media with monoclinic symmetry. The first model is formed by two different nonorthogonal sets of rotationally invariant vertical fractures in an isotropic host rock; the other contains a single set of fractures with microcorrugated faces.

In monoclinic media with two fracture sets, the shear-wave polarizations at vertical incidence and the orientation of the NMO ellipses of pure modes in a horizontal layer are controlled by the fracture azimuths as well as by their compliances. While the *S*-wave polarization directions depend only on the tangential compliances, the axes of the *P*-wave NMO ellipse are also influenced by the normal compliances and therefore have a different orientation. This yields an apparent discrepancy between the principal anisotropy directions obtained using *P* and *S* data that does not exist in orthorhombic media. By first using the weak-anisotropy approximation for the effective anisotropic parameters and then inverting the exact equations, we devise a complete fracture characterization procedure based on the vertical velocities of the *P*- and two split *S*-waves (or converted *PS*-waves) and their NMO ellipses from a horizontal reflector. Our algorithm yields the azimuths and compliances of both fracture systems as well as the *P*- and *S*-wave velocities in the isotropic background medium.

In the model with a single set of microcorrugated fractures, monoclinic symmetry stems from the coupling between the normal and tangential (to the fracture faces) slips, or jumps in displacement. We demonstrate that for this model the shear-wave splitting coefficient at vertical incidence varies with the fluid content of the fractures. Although conventional fracture models that ignore microcorrugation predict no such dependence, our conclusions are supported by experimental observations showing that shear-wave splitting for dry cracks may be substantially greater than that for fluid-filled ones.

INTRODUCTION

This work completes our series of three papers on seismic characterization of naturally fractured reservoirs. The first two papers are devoted to the model with a single system of rotationally invariant fractures in an isotropic background (Bakulin et al. 2000a; hereafter referred to as part I) and to fractured models with orthorhombic symmetry (Bakulin et al. 2000b; part II). Parts I and II contain a detailed review of recent publications on fracture characterization that is not repeated here. All three papers strive to build a bridge between rock physics theories of fractured media and seismic methods of fracture detection. They also attempt to develop efficient fracture characterization methodologies based on surface reflection data.

Theoretical tools (the so-called effective medium theories) for modeling the seismic response of fractured media have existed since the early 1980s (e.g., Schoenberg, 1980, 1983; Hudson, 1980, 1981, 1988; Thomsen, 1995). In particular, Schoenberg (1980, 1983) and Schoenberg and Muir (1989) suggest treating fractures as highly compliant surfaces inside a solid host rock. According to their linear-slip theory, the effective compliance of a rock mass with one or several fracture sets can be found as the sum of the compliances of the host (background) rock and those of all the fractures. Then the background and fracture parameters can be related to the effective Thomsen-type anisotropic coefficients, which govern the influence of anisotropy on various seismic signatures.

Manuscript received by the Editor June 16, 1999; revised manuscript received March 3, 2000.
*Formerly St. Petersburg State University, Department of Geophysics, St. Petersburg, Russia. Presently Schlumberger Cambridge Research, High Cross, Madingley Road, Cambridge CB 3 0EL, England. E-mail: bakulin@cambridge.scr.slb.com.
‡Colorado School of Mines, Center for Wave Phenomena, Department of Geophysics, Golden, Colorado 80401-1887. E-mail: vgrechka@dix.mines.edu; ilya@dix.mines.edu.

This formalism can be used to invert seismic signatures for the fracture compliances and to make inferences about the physical properties of the fracture network. (Schoenberg and Douma (1988) and part I show that fracture compliances effectively absorb such information about the microstructure of fractures as their shape, possible interaction, partial saturation, the presence of equant porosity, etc. This information cannot be obtained unambiguously from seismic data alone.)

In part I we implement these ideas for transversely isotropic media with a horizontal symmetry axis (HTI) formed by a single set of vertical rotationally invariant fractures. A system of vertical fractures in a VTI (transversely isotropic with a vertical symmetry axis) background or two orthogonal fracture sets in an isotropic host rock lead to a medium of orthorhombic symmetry examined in part II. Further complications introduced into the model may lower the symmetry of the effective medium to monoclinic. First experimental evidence of monoclinic symmetry in the subsurface is provided by Winterstein and Meadows (1991), who analyze walkaway vertical seismic profiling (VSP) data over a fractured reservoir.

Here, we discuss two types of fracture-induced monoclinic media. The first model contains two different nonorthogonal sets of rotationally invariant fractures in an isotropic background. We prove that all fracture parameters of the effective monoclinic medium with a horizontal symmetry plane can be estimated using the vertical and NMO velocities of the P- and two split S (or PS)-waves reflected from horizontal interfaces. It should be emphasized that shear-wave data alone do not contain enough information to constrain the model parameters (Liu et al., 1993). Also, we confirm the result of Grechka et al. (2000) that the polarization directions of the vertically propagating shear waves generally are not aligned with the axes of the P-wave NMO ellipse (which cannot happen in the higher symmetry HTI or orthorhombic media). A similar conclusion is drawn by Sayers (1998) who examines the azimuthal variation of the P-wave phase-velocity function in monoclinic media. This gives a plausible theoretical explanation for the discrepancies in the fracture orientation estimated from P- and S-wave data by Pérez et al. (1999).

The second monoclinic model examined here has a vertical symmetry plane and consists of a single set of microcorrugated (rotationally noninvariant) fractures in an isotropic matrix. We derive the shear-wave splitting coefficient as a function of the compliances and show that it is substantially different for fluid-filled and dry fractures.

TWO SETS OF VERTICAL FRACTURES

Effective elastic parameters

Within the framework of the linear-slip theory, the effective compliance matrix $\mathbf{s}$ of a rock with multiple fracture sets can be determined as the sum of the compliance $\mathbf{s}_b$ of the background medium and the fracture compliances $\mathbf{s}_f$ (Nichols et al., 1989; Schoenberg and Muir, 1989; Molotkov and Bakulin, 1997; Bakulin and Molotkov, 1998). Considering two different arbitrarily oriented fracture sets with the compliances $\mathbf{s}_{f1}$ and $\mathbf{s}_{f2}$ in a purely isotropic background, we can represent the effective compliance as

$$\mathbf{s} = \mathbf{s}_b + \mathbf{s}_{f1} + \mathbf{s}_{f2} \equiv \mathbf{c}^{-1}, \tag{1}$$

where $\mathbf{c}$ is the stiffness matrix of the effective medium. The compliance $\mathbf{s}_b$ of the isotropic background, written in terms of the Lamé parameters λ and μ, has the form

$$\mathbf{s}_b = \begin{pmatrix} \frac{\lambda+\mu}{\mu(3\lambda+2\mu)} & -\frac{\lambda}{2\mu(3\lambda+2\mu)} & -\frac{\lambda}{2\mu(3\lambda+2\mu)} & 0 & 0 & 0 \\ -\frac{\lambda}{2\mu(3\lambda+2\mu)} & \frac{\lambda+\mu}{\mu(3\lambda+2\mu)} & -\frac{\lambda}{2\mu(3\lambda+2\mu)} & 0 & 0 & 0 \\ -\frac{\lambda}{2\mu(3\lambda+2\mu)} & -\frac{\lambda}{2\mu(3\lambda+2\mu)} & \frac{\lambda+\mu}{\mu(3\lambda+2\mu)} & 0 & 0 & 0 \\ 0 & 0 & 0 & \frac{1}{\mu} & 0 & 0 \\ 0 & 0 & 0 & 0 & \frac{1}{\mu} & 0 \\ 0 & 0 & 0 & 0 & 0 & \frac{1}{\mu} \end{pmatrix}. \tag{2}$$

Assuming that both fracture sets are rotationally invariant, their matrices $\mathbf{s}_{fi}$ $(i = 1, 2)$ can be described by the normal and tangential (with respect to the crack faces) compliances K_{Ni} and K_{Ti}. If the normal $\mathbf{n}_i$ to the ith fracture set points in the direction of the x_1-axis, the compliance matrix is given by (Schoenberg and Douma, 1988; Schoenberg and Sayers, 1995; part I)

$$\mathbf{s}_{fi}^{x_1} = \begin{pmatrix} K_{Ni} & 0 & 0 & 0 & 0 & 0 \\ 0 & 0 & 0 & 0 & 0 & 0 \\ 0 & 0 & 0 & 0 & 0 & 0 \\ 0 & 0 & 0 & 0 & 0 & 0 \\ 0 & 0 & 0 & 0 & K_{Ti} & 0 \\ 0 & 0 & 0 & 0 & 0 & K_{Ti} \end{pmatrix}. \tag{3}$$

Rotation of the fracture normal by the angle ϕ_i around the x_1-axis changes the matrix $\mathbf{s}_{fi}$ according to the so-called Bond transformation,

$$\mathbf{s}_{fi} = \mathbf{N}(\phi_i)\, \mathbf{s}_{fi}^{x_1}\, \mathbf{N}^{\mathbf{T}}(\phi_i), \tag{4}$$

where the 6×6 matrix $\mathbf{N}$ ($\mathbf{N}^{\mathbf{T}}$ is the transpose) is explicitly written in Winterstein (1990). The exact expressions for $\mathbf{s}_{fi}$, taken

from Schoenberg et al. (1999), are given in Appendix A. It seems to be natural to choose the coordinate frame in such a way that one of the fracture sets is orthogonal to the axis x_1 (or x_2), as is done by Liu et al. (1993). As we discuss below, however, a simpler effective stiffness matrix can be obtained by aligning the horizontal coordinate axes with the polarization directions of the vertically traveling S-waves. In this case, neither fracture system is orthogonal to one of the horizontal coordinate directions.

Equations (1)–(4) make it possible to compute the compliance (**s**) and stiffness (**c**) matrices of the effective medium formed by two vertical fracture sets in an isotropic background. Analysis of the compliance matrix [see equations (A-1)–(A-9) for a single fracture set] shows that this medium is monoclinic with a horizontal symmetry plane. Below, we discuss the inversion of the effective anisotropic coefficients of monoclinic media for the fracture parameters.

Anisotropic coefficients of monoclinic media

Dimensionless anisotropic parameters, first introduced by Thomsen (1986) for VTI media, proved to be extremely useful in seismic velocity analysis and inversion. The main advantage of Thomsen's notation is in capturing the combinations of the stiffness coefficients responsible for a wide range of seismic signatures (Tsvankin, 1996). Thomsen-style notation for HTI media was introduced by Rüger (1997) and Tsvankin (1997a). (In part I we discuss the inversion of the anisotropic coefficients $\epsilon^{(V)}$, $\delta^{(V)}$, and $\gamma^{(V)}$ of fracture-induced HTI media for the fracture compliances.) Tsvankin (1997b) shows that orthorhombic media can be conveniently described by seven anisotropic coefficients and two vertical velocities (of the P- and one of the split S-waves), with a total of only six parameters fully responsible for the P-wave kinematics. Tsvankin's notation simplifies the expressions for azimuthally varying NMO velocities in orthorhombic media (Grechka and Tsvankin, 1998) and helps to identify the subset of the medium parameters that can be determined using P-wave surface reflection data (Grechka and Tsvankin, 1999).

An extension of Thomsen parameters to monoclinic media is suggested by Grechka et al. (2000). They note that the expression for NMO ellipses of P- and S-waves from horizontal reflectors take a particularly simple form if the horizontal coordinate axes x_1 and x_2 coincide with the polarization directions of the vertically propagating split shear waves S_1 and S_2. In this natural coordinate frame the stiffness coefficient c_{45} vanishes (Helbig, 1994; Mensch and Rasolofosaon, 1997),

$$c_{45} = 0, \tag{5}$$

and the number of independent stiffnesses reduces from 13 to 12.

Grechka et al. (2000) replace the stiffness elements with the vertical velocities of P-waves (V_{P0}) and one of the S-waves (V_{S0}) and 10 anisotropic coefficients denoted as $\epsilon^{(1,2)}$, $\delta^{(1,2,3)}$, $\gamma^{(1,2)}$, and $\zeta^{(1,2,3)}$ (Appendix B). These parameters can be divided into two different groups. The first contains the vertical velocities and the ϵ, δ, and γ coefficients, which are defined exactly in the same way as Tsvankin's (1997b) parameters for orthorhombic media. These nine quantities mainly control the semiaxes of the NMO ellipses of waves P, S_1, and S_2 reflected from horizontal interfaces. The second group includes the three ζ coefficients responsible for the rotation of the NMO ellipses with respect to the coordinate axes (Grechka et al., 2000). The parameter $\zeta^{(3)}$ determines the orientation of the P-wave NMO ellipse, whereas $\zeta^{(1)}$ and $\zeta^{(2)}$ govern the rotations of the S_1- and S_2-ellipses, respectively [see equations (B-10)–(B-12)]. This definition of the ζ coefficients distinguishes the notation of Grechka et al. (2000) from the Thomsen-style parameterization of arbitrary anisotropic media introduced by Mensch and Rasolofosaon (1997).

Estimation of fracture parameters

Grechka et al. (2000) show that 11 (out of 12) parameters of monoclinic media [V_{P0}, V_{S0}, $\epsilon^{(1,2)}$, $\delta^{(1,2)}$, $\gamma^{(1,2)}$, and $\zeta^{(1,2,3)}$] can be estimated in a stable way using the vertical velocities and NMO ellipses from horizontal reflectors of the P- and two split S-waves. If the survey is acquired with P-wave sources, pure shear reflections can be replaced by the converted waves PS_1 and PS_2; this option is especially practical for offshore data.

Our goal is to demonstrate that the 11 effective quantities listed above can be inverted for the following physical parameters of the model: the P- and S-wave velocities V_P and V_S in the isotropic background, the azimuths ϕ_1 and ϕ_2 of the normals to the fracture faces, and dimensionless fracture weaknesses denoted by Δ_{Ni} and Δ_{Ti} ($i = 1, 2$). The weaknesses are related to the fracture compliances K_{Ni} and K_{Ti} as (Hsu and Schoenberg, 1993; part I)

$$\Delta_{Ni} = \frac{(\lambda + 2\mu)\, K_{Ni}}{1 + (\lambda + 2\mu)\, K_{Ni}} \quad \text{and} \quad \Delta_{Ti} = \frac{\mu\, K_{Ti}}{1 + \mu\, K_{Ti}}, \qquad (i = 1, 2), \tag{6}$$

where Δ_{Ni} and Δ_{Ti} are always positive and vary from zero (no fracturing) to unity (extreme degree of fracturing).

For isolated penny-shaped cracks, vanishing values of the ratio Δ_{Ni}/Δ_{Ti} correspond to fluid-filled fractures, whereas $\Delta_{Ni}/\Delta_{Ti} \approx (\lambda + 2\mu)/\mu$ (or $K_{Ni} \approx K_{Ti}$) indicate that the cracks are dry. Also, regardless of the type of crack infill, the tangential weakness Δ_{Ti} is close to twice the crack density e_i (part I). If we ignore the influence of one fracture system on the other (a reasonable assumption for small crack density), these relations hold for the weaknesses of each system.

Following Grechka et al. (2000), we choose the axis x_1 to coincide with the polarization direction of the fast shear wave S_1 at vertical incidence (Figure 1). In this coordinate frame, c_{45} vanishes [equation (5)], providing an additional constraint for the fracture parameters. This constraint can be obtained by analyzing the nonzero elements of the effective compliance matrix **s** [equation (1)] and the matrices $\mathbf{s}_b$ [equation (2)], $\mathbf{s}_{f1}$, and $\mathbf{s}_{f2}$ [equations (A-1)–(A-9)]. Since s_{44}, s_{45}, and s_{55} are the only nonzero elements of the fourth and fifth columns and the fourth and fifth rows of **s**, the inverse (stiffness) matrix **c** has a block

$$\begin{pmatrix} c_{44} & c_{45} \\ c_{45} & c_{55} \end{pmatrix} = \begin{pmatrix} s_{44} & s_{45} \\ s_{45} & s_{55} \end{pmatrix}^{-1}.$$

Hence, $c_{45} = 0$ requires that

$$s_{45} = 0, \tag{7}$$

which can be satisfied only if [see equations (1), (2), and (A-7)]

$$K_{T1}\sin 2\phi_1 + K_{T2}\sin 2\phi_2 = 0. \tag{8}$$

Replacing the compliances with the weaknesses [equation (6)] yields

$$\frac{\Delta_{T1}}{1-\Delta_{T1}}\sin 2\phi_1 + \frac{\Delta_{T2}}{1-\Delta_{T2}}\sin 2\phi_2 = 0. \tag{9}$$

Thus, we have a total of 12 equations [11 monoclinic parameters V_{P0}, V_{S0}, $\epsilon^{(1,2)}$, $\delta^{(1,2)}$, $\gamma^{(1,2)}$, and $\zeta^{(1,2,3)}$ plus constraint (9)] to be solved for eight unknowns [V_P, V_S, Δ_{Ni}, Δ_{Ti}, and ϕ_i ($i = 1, 2$)]. The nonlinear relations between the anisotropic coefficients and fracture parameters make it necessary to apply numerical methods and study the uniqueness of the solution. As shown below, our inversion algorithm converges toward values close to the actual model parameters, given a reasonable magnitude of errors in the input data.

Equations (8) and (9) allow us to make two important conclusions about the fracture orientation even prior to the inversion. First, equation (9) can be satisfied only if the fracture azimuths ϕ_1 and ϕ_2 (assumed to lie between $-\pi/2$ and $\pi/2$) have opposite signs because both Δ_{T1} and Δ_{T2} are nonnegative (Figure 1). Therefore, the angle between the normals (and the two crack systems themselves) can be found as $\phi_1 - \phi_2$; the absolute values of ϕ_1 and ϕ_2 are equal only if $\Delta_{T1} = \Delta_{T2}$.

Second, equation (8) indicates that for a fixed angle between the fractures, the azimuths ϕ_1 and ϕ_2 are controlled only by the ratio of the tangential compliances K_{T1}/K_{T2}. The shear-wave polarization directions bisect the angles between the fractures if $K_{T1} = K_{T2}$. To find the fracture orientation relative to the shear-wave polarization directions when $K_{T1} \neq K_{T2}$, we need to supplement equation (8) with the condition

$$c_{55} > c_{44}. \tag{10}$$

Inequality (10) ensures that the fast shear wave S_1 is polarized along the x_1-axis (Figure 1). Using equations (1)–(4), we can rewrite condition (10) in the form

$$K_{T1}\cos 2\phi_1 + K_{T2}\cos 2\phi_2 < 0. \tag{11}$$

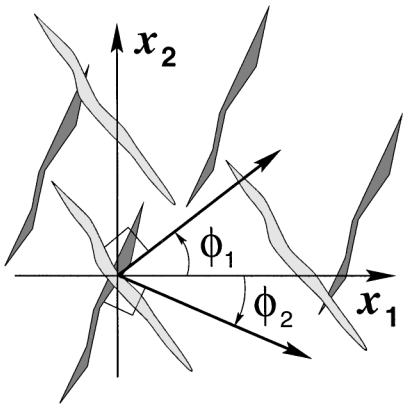

FIG. 1. Two sets of parallel vertical fractures form an effective monoclinic medium. The fracture normals make the angles ϕ_1 and ϕ_2 with the axis x_1 that coincides with the polarization direction of the vertically traveling S_1-wave. To define ϕ_1 and ϕ_2 in a unique fashion, we assume that $-\pi/2 \le \phi_1 < \pi/2$ and $-\pi/2 < \phi_2 \le \pi/2$.

Combined with equation (8), inequality (11) unambiguously defines the directions of both fracture sets for given values of K_{T1}, K_{T2}, and the angle $\phi_1 - \phi_2$.

Let us assume that the first fracture set has a higher tangential compliance ($K_{T1} > K_{T2}$). Analysis of equations (8) and (11) shows that in this case the normal to the first fracture set lies within the interval $\pi/4 < \phi_1 < 3\pi/4$. Hence, the polarization direction of the fast (S_1) shear wave (i.e., the x_1-axis) is always closer to the strike of the more compliant fractures. According to the quantitative estimates in Figure 2, for $K_{T1}/K_{T2} > 3$ the S_1-polarization direction does not deviate by more than 10° from the strike of the first fracture system. In the limit of $K_{T1} \gg K_{T2}$, the medium becomes effectively HTI, and the polarization of the S_1-wave is parallel to the first fracture set; this result is well known for horizontal transverse isotropy (e.g., Winterstein, 1990).

Weak-anisotropy approximation.—If the fracture density is small and the weaknesses $\Delta_{Ni} \ll 1$ and $\Delta_{Ti} \ll 1$, the effective medium is weakly anisotropic. In this case, it is possible to simplify the expressions for the anisotropic coefficients by linearizing them in the weaknesses Δ_{Ni} and Δ_{Ti} (Appendix C). Equations (C-1)–(C-11) show that all ϵ, δ, and γ coefficients are even functions of the fracture azimuths ϕ_1 and ϕ_2, and information about the signs of the azimuths can be obtained only from the ζ coefficients. Since $\zeta^{(1,2,3)}$ determine the rotation of the P- and S-wave NMO ellipses with respect to the shear-wave polarization directions (Grechka et al., 2000), this result indicates the importance of carefully measuring the orientation of the elliptical axes.

The linearized expressions (C-1)–(C-11) can be used to estimate all fracture parameters following, for instance, the algorithm outlined in Appendix D. To check the accuracy of the weak-anisotropy approximation, we computed the exact anisotropic coefficients for the fracture parameters given in Table 1 and carried out the inversion using the equations from Appendix D. For typical moderate values of the tangential

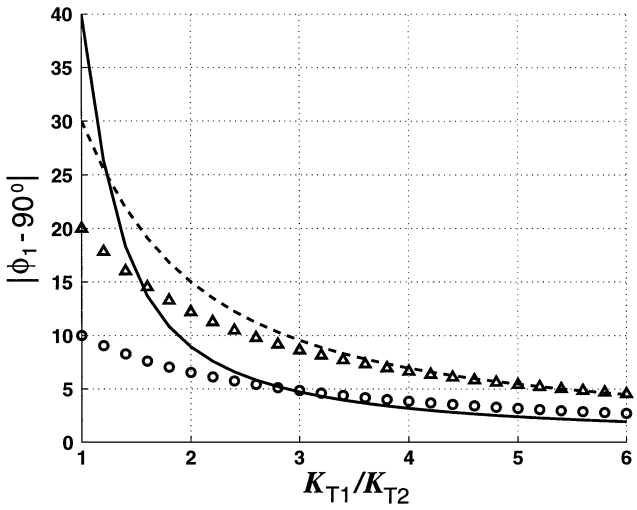

FIG. 2. Azimuth of first fracture system ($|\phi_1 - 90^\circ|$) as a function of the ratio of the tangential compliances K_{T1}/K_{T2}. Each curve corresponds to a different angle between the fracture systems: $\phi_1 - \phi_2 = 20^\circ$ (circles), 40° (triangles), 60° (dashed line), and 80° (solid line).

compliances for both fractures systems (if the fractures are penny-shaped, the crack densities are $e_1 \approx \Delta_{T1}/2 = 0.06$ and $e_2 \approx \Delta_{T2}/2 = 0.10$), our approximation leads to noticeable errors in two weaknesses (Δ_{T1} and Δ_{N2}). However, it can still be used to obtain a good initial guess for the nonlinear inversion.

Special case: Equal tangential weaknesses.—It is instructive to examine the special case of equal tangential weaknesses of the two fracture systems:

$$\Delta_{T1} = \Delta_{T2} \equiv \Delta_T. \tag{12}$$

Then, as follows from equation (9),

$$\phi_1 = -\phi_2 \equiv \phi, \tag{13}$$

and the S_1-wave polarization direction bisects the angle between the fracture sets (see Figure 2 for $K_{T1} = K_{T2}$, which corresponds to $\Delta_{T1} = \Delta_{T2}$). Substituting relations (12) and (13) into equations (C-1)–(C-11), we obtain equations (E-3)–(E-13), which can be inverted for the fracture parameters in a relatively straightforward fashion. The results of Appendix E indicate that the fracture azimuth ϕ and the weaknesses Δ_T, Δ_{N1}, and Δ_{N2} can be found just from the vertical velocities of the P- and S-waves and the P-wave NMO ellipse; the shear-wave NMO ellipses provide redundant information.

If the tangential weaknesses of the two fracture sets are equal, the orientations of the pure-mode NMO ellipses are related in a simple way to the fracture azimuths. For instance, the azimuth θ_P of the semimajor axis of the P-wave NMO ellipse can be written in the weak-anisotropy approximation as (Grechka et al., 2000)

$$\tan 2\theta_P = \frac{2\zeta^{(3)}}{\delta^{(2)} - \delta^{(1)}}. \tag{14}$$

Substituting equations (E-7), (E-8), and (E-13) into equation (14), we find

$$\tan 2\theta_P = A_P \tan 2\phi, \tag{15}$$

where

$$A_P = \frac{(\Delta_{N2} - \Delta_{N1})(1 - 2g)}{(\Delta_{N1} + \Delta_{N2})(1 - 2g) + 2\Delta_T}. \tag{16}$$

Note that $|A_P| \le 1$, which implies that the axes of the P-wave NMO ellipse deviate from both fracture azimuths (except for the special case of orthogonal fractures discussed below). Also, if $\Delta_{N2} \neq \Delta_{N1}$, the angle $\theta_P \neq 0$ and the P-wave ellipse is rotated with respect to the polarization directions of the vertically propagating shear waves, as noted by Grechka et al. (2000) (see also Sayers, 1998). This may explain the discrepancies in the fracture orientation estimated from the P-wave NMO ellipse and S-wave polarizations described by Pérez et al. (1999). The same conclusion is true for the NMO ellipses of the S_1- and S_2-waves whose rotation angles are determined by the parameters $\zeta^{(1)}$ and $\zeta^{(2)}$ (Grechka et al., 2000). As follows from equations (E-11) and (E-12) for the fracture-induced monoclinic model, $\zeta^{(1)} \neq 0$ and $\zeta^{(2)} \neq 0$.

If the two fracture systems are identical [i.e., $\Delta_{N1} = \Delta_{N2}$ in addition to $\Delta_{T1} = \Delta_{T2}$], the axes of the P-wave NMO ellipse are aligned with the shear-wave polarization directions ($A_P = \theta_P = 0$). In this case, the medium becomes orthorhombic, and S-wave polarization vectors (which bisect the fractures) lie in the vertical symmetry planes of the model. For $\Delta_{N1} = \Delta_{N2}$, all three ζ coefficients vanish, so the shear-wave NMO ellipses are cooriented with the P-wave ellipse.

Another special case of orthorhombic symmetry is that of different but orthogonal fracture sets ($2\phi = 90^\circ$). If only the normal weaknesses Δ_{N1} and Δ_{N2} are different (but $\Delta_{T1} = \Delta_{T2}$), shear waves do not split at vertical incidence and have no defined polarization directions (part II).

For monoclinic media, the axes of the P-wave NMO ellipse and the polarization vectors of the vertically traveling S-waves are parallel only if the ratio of the tangential and normal compliances is the same for both fracture systems (i.e., $\zeta^{(3)} = 0$ if $K_{N1}/K_{T1} = K_{N2}/K_{T2}$ or $\Delta_{N1}/\Delta_{T1} = \Delta_{N2}/\Delta_{T2}$). This result, valid only in the weak anisotropy approximation, can be obtained from equations (8), (9), and (C-11). For example, $\zeta^{(3)} = 0$ if the normal and tangential compliances are equal to each other, which agrees with the result of Sayers (1998).

Table 1. Comparison of the actual fracture parameters with those estimated from the exact anisotropic coefficients using the linearized formulas from Appendix D.

Parameter	V_S/V_P	Δ_{N1}	Δ_{T1}	ϕ_1	Δ_{N2}	Δ_{T2}	ϕ_2
Actual	0.5	0.25	0.12	30°	0.00	0.20	−13°
Estimated	0.5	0.20	0.04	40°	0.08	0.22	−5°

Arbitrary fracture sets.—The main significance of the linearized approximations for the fracture parameters is in providing insight into the behavior of the anisotropic coefficients and a good initial model for the inversion procedure. Here we discuss the inversion of the anisotropic parameters for the fracture compliances and orientations based on the exact equations (1)–(4) for the stiffnesses and the definitions from Appendix B. We assume that the quantities V_{P0}, V_{S0}, $\epsilon^{(1,2)}$, $\delta^{(1,2)}$, $\gamma^{(1,2)}$, and $\zeta^{(1,2,3)}$ have been estimated from the vertical and NMO velocities of the P- and split S-waves (or converted PS-waves). To examine the stability of the inversion algorithm, we introduce errors in all quantities [similar to those shown in Figures 2 and 4 in Grechka et al. (2000)] caused by Gaussian noise with a variance of 2% added to the NMO velocities. The variances of the errors in the effective parameters are as follows: 2% in V_{P0} and V_{S0}, 0.01 in $\zeta^{(1)}$ and $\zeta^{(2)}$, and 0.03 in all other anisotropic coefficients. The fracture parameters that give the best fit to the error-contaminated values of the vertical velocities and anisotropic coefficients are found by minimization using the simplex method.

Figure 3 displays typical inversion results for the V_P/V_S ratio in the isotropic background and weaknesses Δ_{Ni} and Δ_{Ti}. The standard deviation in the estimated V_S/V_P ratio (3.1%) is somewhat higher than that in the input vertical velocities V_{P0} and V_{S0} but is still quite acceptable. The errors in the weaknesses Δ_{Ti} are about twice as large as those in the input anisotropic coefficients. This error amplification can be understood from the weak-anisotropy approximations (D-6) and (D-8), which indicate that Δ_{Ti} are derived from the γ coefficients multiplied by a factor of 2; similar results are obtained for models with one system of fractures in parts I and II.

The accuracy of the inverted normal weaknesses Δ_{Ni} is even lower than that of Δ_{Ti}. This can also be explained using the weak-anisotropy approximations (C-1)–(C-11), which contain terms in the form $\Delta_{Ti} \pm a\Delta_{Ni}$ with $|a| < 1$. Therefore, the same errors in the input anisotropic coefficients can be compensated by greater variations in Δ_{Ni} compared to those in Δ_{Ti}. Even though the errors in Δ_{Ni} are rather significant, Figure 3 shows that we can still distinguish between dry fractures [the first system with $K_{N1} \approx K_{T1}$ or $\Delta_{T1}(1-\Delta_{N1}) \approx g\Delta_{N1}(1-\Delta_{T1})$] and fluid-filled ones with $\Delta_{N2} \approx 0$. The unphysical values $\Delta_{N2} < 0$ appear in Figure 3 because random errors added to the data may produce anisotropic coefficients that do not correspond to any fractured media.

MICROCORRUGATED FRACTURES AND FLUID-DEPENDENT SHEAR-WAVE SPLITTING

Shear-wave splitting at vertical incidence traditionally has been regarded as the most reliable measure of fracture intensity for a set of parallel vertical fractures embedded in an isotropic or VTI host rock. The fractional difference between the *S*-wave vertical velocities V_{S1} and V_{S2} is expressed through the so-called shear-wave splitting parameter $\gamma^{(S)}$, defined as

$$\gamma^{(S)} \equiv \frac{V_{S1}^2 - V_{S2}^2}{2V_{S2}^2} \approx \frac{V_{S1} - V_{S2}}{V_{S2}}. \qquad (17)$$

It has been common knowledge among researchers working on fracture characterization that $\gamma^{(S)}$ depends only on the crack density and does not contain information about the fluid content of the fractures. This conclusion seems to have been confirmed both theoretically (Hudson, 1981; Thomsen, 1995) and experimentally (e.g., Martin and Davis, 1987; Winterstein and Meadows, 1991). On the other hand, Guest et al. (1998) present a case study where the splitting parameter for gas-filled cracks proves to be significantly higher than that for brine-filled ones, which clearly contradicts the existing understanding. Here, we give a possible theoretical explanation of these observations by obtaining the effective parameters of a fracture set with microcorrugated faces. The idea of the theory is to allow the coupling between the tangential slip along fracture faces (responsible for shear-wave splitting) and the normal slip known to depend on the fluid content.

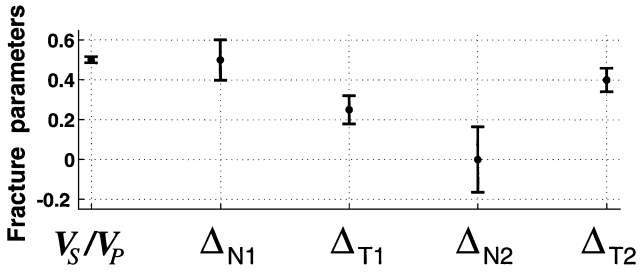

FIG. 3. Results of the inversion for the parameters of two fracture systems and the background velocities. The dots mark the actual values of the fracture parameters; the bars correspond to ± one standard deviation in the inverted quantities. Not shown are the standard deviations in the estimated background velocities V_P and V_S (2.0% and 2.5%, respectively) and in the fracture azimuths (9°; the actual values are $\phi_1 = 30°$ and $\phi_2 = -12.8°$).

Linear-slip model for fractures with microcorrugated faces

As in the previous section, our analysis is based on the linear-slip theory of Schoenberg (1980), Schoenberg and Muir (1989), and Schoenberg and Sayers (1995). For simplicity, we examine a single system of parallel fractures with the normal $\mathbf{n} = [1, 0, 0]$ in an isotropic background medium. The matrix of the excess fracture compliance in this case has the form (Schoenberg and Douma, 1988; part I)

$$\mathbf{s}_f = \begin{pmatrix} K_N & 0 & 0 & 0 & K_{NV} & K_{NH} \\ 0 & 0 & 0 & 0 & 0 & 0 \\ 0 & 0 & 0 & 0 & 0 & 0 \\ 0 & 0 & 0 & 0 & 0 & 0 \\ K_{NV} & 0 & 0 & 0 & K_V & K_{VH} \\ K_{NH} & 0 & 0 & 0 & K_{VH} & K_H \end{pmatrix}, \qquad (18)$$

where K_N is the normal fracture compliance that relates the jump of the displacement normal to the fracture (i.e., the normal slip) to the normal stress in the direction [1, 0, 0]. The values K_V and K_H are the tangential compliances relating the slips and stresses in the vertical [0, 0, 1] (K_V) and horizontal [0, 1, 0] (K_H) directions. The compliance K_{NV} couples the normal slip to the tangential vertical stress or, equivalently, the tangential slip in the direction [0, 0, 1] to the normal stress. Likewise, the compliances K_{NH} and K_{VH} couple the horizontal stress in the [0, 1, 0] direction to the normal and vertical slips.

The conventional conclusion about the shear-wave splitting coefficient $\gamma^{(S)}$ being independent of fracture infill is based on the *assumption* that the normal and tangential slips are decoupled ($K_{NV} = K_{NH} = K_{VH} = 0$) and the matrix (18) is diagonal. An alternative model of cracks with microcorrugated faces (see Figure 4) is suggested by Schoenberg and Douma (1988). Since the stresses in either the normal (x_1) or vertical

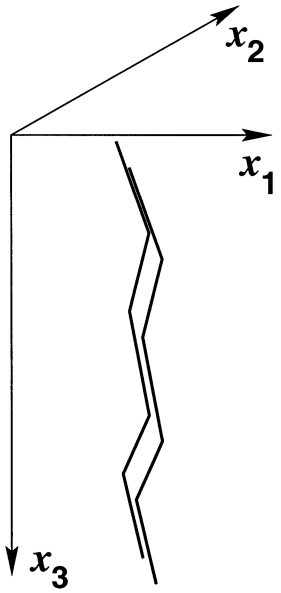

FIG. 4. Cross-section of a vertical fracture with microcorrugated faces. This microstructure leads to the coupling between the normal and tangential slips (after Schoenberg and Douma, 1988).

(x_3) direction applied to such a fracture produce slips in both x_1- and x_3-directions, the compliance component K_{NV} must be nonzero. In contrast, the component K_{VH} can always be set to zero by the appropriate rotation of the coordinate system (Berg et al., 1991). Below, we show that fractures characterized by the compliances

$$K_{NH} = K_{VH} = 0 \quad \text{and} \quad K_{NV} \neq 0 \tag{19}$$

cause infill-dependent shear-wave splitting.

Effective model of fractured media

If a fracture system with the compliances described by equations (18) and (19) is embedded in an isotropic rock, the effective stiffness matrix has the form [see equation (1)]

$$\mathbf{c}^{-1} = \mathbf{s}_b + \mathbf{s}_f, \tag{20}$$

where the background compliance matrix $\mathbf{s}_b$ is given by equation (2). Evaluating the components of the matrix $\mathbf{c}$ yields

$$\mathbf{c} = \begin{pmatrix} c_{11} & c_{12} & c_{12} & 0 & c_{15} & 0 \\ c_{12} & c_{33} & c_{23} & 0 & c_{35} & 0 \\ c_{12} & c_{23} & c_{33} & 0 & c_{35} & 0 \\ 0 & 0 & 0 & c_{44} & 0 & 0 \\ c_{15} & c_{35} & c_{35} & 0 & c_{55} & 0 \\ 0 & 0 & 0 & 0 & 0 & c_{66} \end{pmatrix}. \tag{21}$$

Equation (21) describes a monoclinic medium with the vertical symmetry plane [x_1, x_3]. The stiffness elements are given by

$$\begin{aligned} c_{11} &= (\lambda + 2\mu)\frac{1 + E_V}{D}, \qquad c_{12} = \lambda\frac{1 + E_V}{D}, \\ c_{15} &= -\sqrt{\mu(\lambda + 2\mu)}\frac{E_{NV}}{D}, \\ c_{33} &= (\lambda + 2\mu)\frac{(1 + E_V)(1 + \nu E_N) - \nu E_{NV}^2}{D}, \\ c_{23} &= \lambda\frac{(1 + 2gE_N)(1 + E_V) - 2gE_{NV}^2}{D}, \\ c_{35} &= -\lambda\frac{\sqrt{g}E_{NV}}{D}, \\ c_{44} &= \mu, \quad c_{55} = \mu\frac{1 + E_N}{D}, \quad \text{and} \quad c_{66} = \frac{\mu}{1 + E_H}, \end{aligned} \tag{22}$$

where

$$D = (1 + E_N)(1 + E_V) - E_{NV}^2, \quad \nu = \frac{4\mu(\lambda + \mu)}{(\lambda + 2\mu)^2},$$
$$g = \frac{\mu}{\lambda + 2\mu},$$

and λ and μ are the Lamé constants of the host rock. The dimensionless compliances E_N, E_V, E_H, and E_{NV} are defined as follows (Hsu and Schoenberg, 1993):

$$E_N = (\lambda + 2\mu)K_N, \tag{23}$$

$$E_V = \mu K_V, \tag{24}$$

$$E_H = \mu K_H, \tag{25}$$

$$E_{NV} = \sqrt{\mu(\lambda + 2\mu)}K_{NV}. \tag{26}$$

The stability condition requires that matrix (18) be nonnegative definite. In our case, this condition implies that all dimensionless compliances E_N, E_V, and E_H are nonnegative and

$$E_N E_V - E_{NV}^2 \geq 0. \tag{27}$$

Shear-wave splitting coefficient

The velocities of the split shear waves traveling in the vertical direction in the monoclinic medium described by equation (21) are given by

$$V_{S1}^2 = \frac{\mu}{\rho} \tag{28}$$

and

$$V_{S2}^2 = \frac{2}{\rho}\frac{c_{33}c_{55} - c_{35}^2}{c_{33} + c_{55} + \sqrt{(c_{33} - c_{55})^2 + 4c_{35}^2}}, \tag{29}$$

where ρ is the density. While the velocity V_{S1} of the fast shear wave is simply equal to the background S-wave velocity, the slower velocity V_{S2} depends on the fracture compliances E_N, E_T, and E_{NV}.

Assuming weak anisotropy ($E_N \ll 1$, $E_T \ll 1$, and $E_{NV} \ll 1$) and keeping the linear and quadratic terms in the dimensionless compliances, we obtain the shear-wave splitting coefficient [equation (17)] as

$$\gamma^{(S)} \approx \frac{E_V}{2} - \frac{E_{NV}^2 g(3 - 4g)}{2(1 - g)}. \tag{30}$$

Equation (30) shows that the coupling between the normal and tangential slips (i.e., $E_{NV} \neq 0$) always *reduces* the value of $\gamma^{(S)}$.

To analyze the influence of fluid content on shear-wave splitting for fractures with microcorrugated faces, we generalize the criterion given by Schoenberg and Sayers (1995) for isolated penny-shaped cracks. They point out that the ratio K_N/K_V may serve as an indicator of fluid saturation because it vanishes for fluid-filled cracks and is equal to unity if the cracks are dry. The result of Schoenberg and Sayers (1995), however, is formulated for $K_{NV} = 0$ and must be modified for microcorrugated fractures.

Let us consider the 2×2 submatrix

$$\tilde{\mathbf{s}}_f = \begin{pmatrix} K_N & K_{NV} \\ K_{NV} & K_V \end{pmatrix} \tag{31}$$

of the compliance matrix (18). Note that the Schoenberg-Sayers criterion for $K_{NV} = 0$ is equivalent to the statement that the fractures are fluid filled if one eigenvalue of $\tilde{\mathbf{s}}_f$ is equal to zero, whereas the fractures are dry if the matrix $\tilde{\mathbf{s}}_f$ has two equal eigenvalues.

We assume that the same relationship between fluid saturation and the eigenvalues of $\tilde{\mathbf{s}}_f$ holds for the more general case with $K_{NV} \neq 0$. To justify this assumption, we recall that the excess compliance matrix $\mathbf{s}_f$ relates the stress applied to the fracture faces to the slip or the jump of the displacement across the fractures (Schoenberg, 1980). The eigenvalues of $\mathbf{s}_f$ or $\tilde{\mathbf{s}}_f$ are the coefficients that relate the magnitudes of the slip and the stress vectors in the principal directions. Intuitively, we expect dry fractures to be equally compliant in all directions (there is no material inside to stiffen them), so the eigenvalues of the fracture compliance matrix are supposed to be equal. In

contrast, fluid-filled fractures are noticeably stiffer in a particular direction where the applied stress tends to squeeze the fluid. Thus, the eigenvalue corresponding to this direction should be significantly smaller than the other eigenvalues.

The submatrix (31) has equal eigenvalues if and only if $K_N = K_V$ and $K_{NV} = 0$, which means [see equation (26)] that

$$E_{NV} = 0. \tag{32}$$

For one of the eigenvalues of $\tilde{\mathbf{s}}_f$ to go to zero, it is required that $K_{NV}^2 = K_N K_V$ or [equations (23), (24), and (26)]

$$E_{NV}^2 = E_N E_V. \tag{33}$$

Since $E_{NV}^2 \le E_N E_V$ [inequality (27)], equations (32) and (33) impose strict bounds on possible absolute values of E_{NV}.

Substituting equations (32) and (33) into equation (30) yields the shear-wave splitting coefficients for dry and fluid-filled cracks:

$$\gamma_{\text{dry}}^{(S)} \approx \frac{E_V}{2} \tag{34}$$

and

$$\gamma_{\text{wet}}^{(S)} \approx \frac{E_V}{2}\left[1 - \frac{E_N g(3-4g)}{1-g}\right]. \tag{35}$$

Hence, for microcorrugated fractures the splitting coefficient is always higher for dry than for fluid-filled fractures, which is consistent with the observations of Guest et al. (1998). Figure 5 illustrates the influence of the dimensionless compliance E_{NV} on the shear-wave splitting coefficient. In this particular example, $\gamma^{(S)}$ decreases by about 30% as the fluid saturation changes from zero ($E_{NV} = 0$) to 100%. Also note that the approximation (30) gives a reasonably accurate qualitative description of $\gamma^{(S)}$.

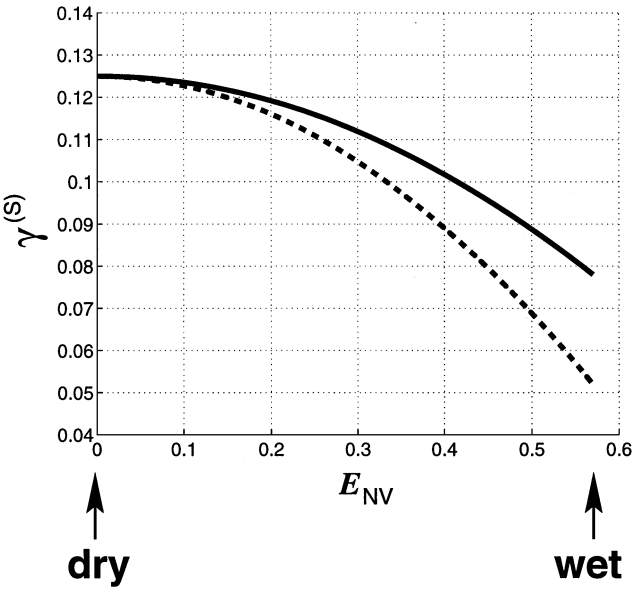

FIG. 5. Shear-wave splitting coefficient $\gamma^{(S)}$ computed from the exact equations (17), (28), and (29) (solid) and the approximation (30) (dashed) as a function of the dimensionless compliance E_{NV}. The model parameters are $g = 0.16$, $E_N = 1.3$, and $E_V = 0.25$.

DISCUSSION AND CONCLUSIONS

The objective of this series of papers was to analyze the dependence of seismic signatures on the physical parameters of fracture networks and to develop fracture characterization algorithms operating with surface seismic data. In part I we considered the simplest model of a single vertical fracture system in a purely isotropic host rock (HTI medium) and showed that the fracture compliances, or the dimensionless fracture weaknesses, are the only quantities that can be unambiguously estimated from seismic data. The microstructure of the fractured formation (e.g., the shape of fractures, their possible interaction, the presence of equant porosity, etc.), however, cannot be evaluated without additional information. For example, if the fractures are known to be penny-shaped and isolated from pore space, the weaknesses give a direct estimate of the crack density and fluid content of the fracture system.

By deriving the relationships between the weaknesses and Thomsen-type anisotropic coefficients, we were able to study the behavior of surface seismic signatures in fracture-induced HTI (part I) and orthorhombic (part II) media. The analytic results for HTI media provided the basis for inversion algorithms designed to estimate the orientation and weaknesses of a vertical fracture set using P-wave reflections alone or a combination of P and converted (PS) data. In part II we extended our parameter estimation methodology to orthorhombic media formed either by a single fracture set in an anisotropic (VTI) host rock or by two orthogonal fracture sets in an isotropic background.

This paper has investigated the inverse problem for an effective monoclinic medium caused by two nonorthogonal sets of rotationally invariant fractures. The weaknesses and azimuths of both fracture systems, along with the velocities in the isotropic background, can be obtained using the vertical velocities and NMO ellipses (from horizontal interfaces) of the P-wave and two split S-waves. In principle, pure S reflections can be replaced in the inversion procedure by the converted (PS) waves. Using the weak anisotropy approximation, we obtain simple, linearized expressions for the fracture parameters, which can serve as a good initial guess for the nonlinear inversion algorithm. Numerical analysis shows that the tangential compliances are generally estimated with a higher accuracy than the normal ones, but the difference between the normal compliances of dry and fluid-filled cracks can still be detected in the presence of noise in the data.

Parameter estimation is particularly convenient to carry out in the natural coordinate frame associated with the polarization directions of the vertically propagating S-waves. These directions are controlled only by the weaknesses Δ_{Ti} tangential to the fracture faces and are independent from the normal weaknesses Δ_{Ni}. In the special case of equal tangential weaknesses $\Delta_{T1} = \Delta_{T2}$, shear-wave polarization directions bisect the angles between the fracture systems, and all fracture weaknesses can be obtained just from the shear-wave splitting coefficient $\gamma^{(S)}$ and the P-wave NMO ellipse. For different tangential compliances, the polarization vector of the fast shear wave deviates toward the strike of the more compliant fracture system.

It is important to note that the axes of the P-wave NMO ellipse generally do not coincide with either the polarization directions of the vertically traveling S-waves or the fracture strike (the same is true for the S-wave NMO ellipses). This

result may explain the observations of Pérez et al. (1999) who find that the predominant fracture orientation obtained using P-wave azimuthal moveout analysis does not agree with that inferred from shear-wave polarizations.

We also examine another monoclinic model that contains a single system of vertical fractures with microcorrugated faces in an isotropic host rock. An important feature of this model is the coupling between the slips (jumps in displacement) in the directions normal and tangential to the fractures. This coupling leads to the dependence of the splitting coefficient $\gamma^{(S)}$ of the vertically traveling S-waves (determined by the tangential slip or tangential weakness) on the fluid content of the fractures (which influences the normal slip). For typical fracture parameters, $\gamma^{(S)}$ may noticeably decrease with fluid saturation, which is consistent with the case study of Guest et al. (1998).

ACKNOWLEDGMENTS

This work was performed during Andrey Bakulin's visit to the Center for Wave Phenomena (CWP), Colorado School of Mines, in 1998. We thank Sean Guest and Cees van der Kolk of Shell for their provocative discussion of the shear-wave splitting coefficient. We are also grateful to members of the A(nisotropy)-Team of CWP for helpful discussions and to Andreas Rüger (Landmark) for his review of the manuscript. The support for this work was provided by the members of the Consortium Project on Seismic Inverse Methods for Complex Structures at CWP and by the U.S. Department of Energy (award #DE-FG03-98ER14908).

REFERENCES

Bakulin, A. V., Grechka, V., and Tsvankin, I., 2000a, Estimation of fracture parameters from reflection seismic data—Part I: HTI model due to a single fracture set: Geophysics, **65**, 1788–1802, this issue.

——— 2000b, Estimation of fracture parameters due to reflection seismic data—Part II: Fractured models with orthorhombic symmetry: Geophysics, **65**, 1803–1817, this issue.

Bakulin, A. V., and Molotkov, L. A., 1998, Effective models of fractured and porous media: St. Petersburg Univ. Press (in Russian).

Berg, E., Hood, J. A., and Fryer, G. J., 1991, Reduction of the general fracture compliance matrix Z to only five independent elements: Geophys. J. Internat., **107**, 703–707.

Grechka, V., and Tsvankin, I., 1998, 3-D description of normal moveout in anisotropic inhomogeneous media: Geophysics, **63**, 1079–1092.

——— 1999, 3-D moveout velocity analysis and parameter estimation for orthorhombic media: Geophysics, **64**, 820–837.

Grechka, V., Contreras, P., and Tsvankin, I., 2000, Inversion of normal moveout for monoclinic media: Geophys. Prosp., **48**, 577–602.

Guest, S., van der Kolk, C., and Potters, H., 1998, The effect of fracture filling fluids on shear-wave propagation: 68th Ann. Internat. Mtg., Soc. Expl. Geophys., Expanded Abstracts, 948–951.

Helbig, K., 1994, Foundations of anisotropy for exploration seismics, *in* Helbig, K., and Treitel, S., Eds., Handbook of geophysical exploration **22**: Pergamon Press.

Hsu, C.-J., and Schoenberg, M., 1993, Elastic waves through a simulated fractured medium: Geophysics, **58**, 964–977.

Hudson, J. A., 1980, Overall properties of a cracked solid: Math. Proc. Camb. Phil. Soc., **88**, 371–384.

——— 1981, Wave speeds and attenuation of elastic waves in material containing cracks: Geophys. J. Roy. Astr. Soc., **64**, 133–150.

——— 1988, Seismic wave propagation through material containing partially saturated cracks: Geophys. J., **92**, 33–37.

Liu, E., Crampin, S., Queen, J. H., and Rizer, W. D., 1993, Behavior of shear waves in rocks with two sets of parallel cracks: Geophys. J. Internat., **113**, 509–517.

Martin, M. A., and Davis, T. L., 1987, Shear-wave birefringence: A new tool for evaluating fractured reservoirs: The Leading Edge, **6**, 22–28.

Mensch, T., and Rasolofosaon, P., 1997, Elastic-wave velocities in anisotropic media of arbitrary symmetry—generalization of Thomsen's parameters ϵ, δ, and γ: Geophys. J. Internat., **128**, 43–64.

Molotkov, L. A., and Bakulin, A.V., 1997, An effective model of a fractured medium with fractures modeled by the surfaces of discontinuity of displacements: J. Math. Sci., **86**, 2735–2746.

Nichols, D., Muir, F., and Schoenberg, M., 1989, Elastic properties of rocks with multiple sets of fractures: 59th Ann. Internat. Mtg., Soc. Expl. Geophys., Expanded Abstracts, 471–474.

Pérez, M. A., Grechka, V., and Michelena, R. J., 1999, Fracture detection in a carbonate reservoir using a variety of seismic methods: Geophysics, **64**, 1266–1276.

Rüger, A., 1997, P-wave reflection coefficients for transversely isotropic models with vertical and horizontal axis of symmetry: Geophysics, **62**, 713–722.

Sayers, C., 1998, Misalignment of the orientation of fractures and the principal axes for P and S waves in rocks containing multiple nonorthogonal fracture sets: Geophys. J. Internat., **133**, 459–466.

Schoenberg, M., 1980, Elastic wave behavior across linear slip interfaces: J. Acoust. Soc. Am., **68**, 1516–1521.

——— 1983, Reflection of elastic waves from periodically stratified media with interfacial slip: Geophys. Prosp., **31**, 265–292.

Schoenberg, M., and Douma, J., 1988, Elastic wave propagation in media with parallel fractures and aligned cracks: Geophys. Prosp., **36**, 571–590.

Schoenberg, M., and Muir, F., 1989, A calculus for finely layered anisotropic media: Geophysics, **54**, 581–589.

Schoenberg, M., and Sayers, C., 1995, Seismic anisotropy of fractured rock: Geophysics, **60**, 204–211.

Schoenberg, M., Dean, S., and Sayers, C., 1999, Azimuth-dependent tuning of seismic waves reflected from fractured reservoirs: Geophysics, **64**, 1160–1171.

Thomsen, L., 1986, Weak elastic anisotropy: Geophysics, **51**, 1954–1966.

——— 1995, Elastic anisotropy due to aligned cracks in porous rock: Geophys. Prosp., **43**, 805–830.

Tsvankin, I., 1996, P-wave signatures and notation for transversely isotropic media: An overview: Geophysics, **61**, 467–483.

——— 1997a, Reflection moveout and parameter estimation for horizontal transverse isotropy: Geophysics, **62**, 614–629.

——— 1997b, Anisotropic parameters and P-wave velocity for orthorhombic media: Geophysics, **62**, 1292–1309.

Winterstein, D. F., 1990, Velocity anisotropy terminology for geophysicists: Geophysics, **55**, 1070–1088.

Winterstein, D. F., and Meadows, M. A., 1991, Shear-wave polarizations and subsurface stress directions at Lost Hills field: Geophysics, **56**, 1331–1348.

APPENDIX A

COMPLIANCE OF AN ARBITRARY ORIENTED VERTICAL FRACTURE SET

The compliance matrix of a fracture system orthogonal to the x_1-axis is given in equation (3). Applying Bond transformation (4) [see Winterstein (1990)] to matrix (3), Schoenberg et al. (1999) obtain the compliance $\mathbf{s}_f$ (for brevity, the number i of the fracture set is omitted) of a fracture system with the normal $\mathbf{n} = [\cos\phi, \sin\phi, 0]$ (Figure A-1). The nonzero elements of the matrix $\mathbf{s}_f$ have the following form:

$$s_{11\,f} = \frac{3K_N + K_T}{8} + \frac{K_N}{2}\cos 2\phi + \frac{K_N - K_T}{8}\cos 4\phi, \tag{A-1}$$

$$s_{12\,f} = \frac{K_N - K_T}{8}(1 - \cos 4\phi), \tag{A-2}$$

$$s_{16\,f} = \frac{K_N}{2}\sin 2\phi + \frac{K_N - K_T}{4}\sin 4\phi, \tag{A-3}$$

$$s_{22\,f} = \frac{3K_N + K_T}{8} - \frac{K_N}{2}\cos 2\phi + \frac{K_N - K_T}{8}\cos 4\phi, \tag{A-4}$$

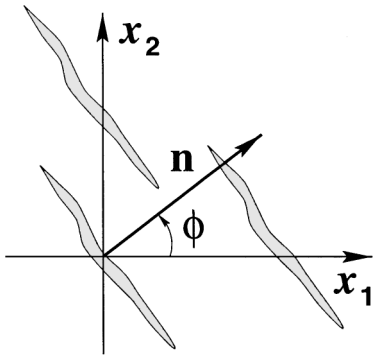

FIG. A-1. Set of vertical fractures with the normal making the angle ϕ with the x_1-axis. The azimuth ϕ is positive in the counterclockwise direction.

$$s_{26\,f} = \frac{K_N}{2}\sin 2\phi - \frac{K_N - K_T}{4}\sin 4\phi, \qquad \text{(A-4)}$$

$$s_{44\,f} = K_T\frac{1-\cos 2\phi}{2}, \qquad \text{(A-5)}$$

$$s_{45\,f} = K_T\frac{\sin 2\phi}{2}, \qquad \text{(A-6)}$$

$$s_{55\,f} = K_T\frac{1+\cos 2\phi}{2}, \qquad \text{(A-7)}$$

$$s_{66\,f} = \frac{K_N + K_T}{2} - \frac{K_N - K_T}{2}\cos 4\phi. \qquad \text{(A-8)}$$

APPENDIX B

ANISOTROPIC PARAMETERS OF MONOCLINIC MEDIA

Using the coordinate frame in which the x_1- and x_2-axes coincide with the polarization directions of the vertically traveling shear waves, Grechka et al. (2000) define anisotropic parameters for monoclinic media by generalizing Thomsen's (1986) and Tsvankin's (1997b) notations for VTI and orthorhombic symmetry systems. Expressions for these parameters in terms of the stiffness coefficients and density ρ are given below.

V_{P0}—P-wave vertical velocity:

$$V_{P0} \equiv \sqrt{\frac{c_{33}}{\rho}}. \qquad \text{(B-1)}$$

V_{S0}—velocity of the vertically traveling S_1-wave, which is polarized in the x_1-direction:

$$V_{S0} \equiv \sqrt{\frac{c_{55}}{\rho}}. \qquad \text{(B-2)}$$

Dimensionless anisotropic parameters:

$$\epsilon^{(1)} \equiv \frac{c_{22} - c_{33}}{2c_{33}}, \qquad \text{(B-3)}$$

$$\delta^{(1)} \equiv \frac{(c_{23} + c_{44})^2 - (c_{33} - c_{44})^2}{2c_{33}(c_{33} - c_{44})}, \qquad \text{(B-4)}$$

$$\gamma^{(1)} \equiv \frac{c_{66} - c_{55}}{2c_{55}}, \qquad \text{(B-5)}$$

$$\epsilon^{(2)} \equiv \frac{c_{11} - c_{33}}{2c_{33}}, \qquad \text{(B-6)}$$

$$\delta^{(2)} \equiv \frac{(c_{13} + c_{55})^2 - (c_{33} - c_{55})^2}{2c_{33}(c_{33} - c_{55})}, \qquad \text{(B-7)}$$

$$\gamma^{(2)} \equiv \frac{c_{66} - c_{44}}{2c_{44}}, \qquad \text{(B-8)}$$

$$\delta^{(3)} \equiv \frac{(c_{12} + c_{66})^2 - (c_{11} - c_{66})^2}{2c_{11}(c_{11} - c_{66})}. \qquad \text{(B-9)}$$

$\zeta^{(1)}$—the parameter responsible for the rotation of S_1-wave NMO ellipse:

$$\zeta^{(1)} \equiv \frac{c_{16} - c_{36}}{2c_{33}}. \qquad \text{(B-10)}$$

$\zeta^{(2)}$—the parameter responsible for the rotation of S_2-wave NMO ellipse:

$$\zeta^{(2)} \equiv \frac{c_{26} - c_{36}}{2c_{33}}. \qquad \text{(B-11)}$$

$\zeta^{(3)}$—the parameter responsible for the rotation of P-wave NMO ellipse:

$$\zeta^{(3)} \equiv \frac{c_{36}}{c_{33}}. \qquad \text{(B-12)}$$

Parameters (B-1)–(B-9) are identical to those defined by Tsvankin (1997b) for the higher-symmetry orthorhombic media. The additional anisotropic coefficients $\zeta^{(1,2,3)}$ are responsible for the rotation of the NMO ellipses of the waves P ($\zeta^{(3)}$), S_1($\zeta^{(1)}$), and S_2($\zeta^{(2)}$) with respect to the coordinate axes. The coefficient $\zeta^{(3)}$ is analogous to the parameter χ_z introduced by Mensch and Rasolofosaon (1997).

APPENDIX C

WEAK-ANISOTROPY APPROXIMATION FOR MEDIA WITH TWO VERTICAL FRACTURE SYSTEMS

Here, we use equations (1)–(4) and the expressions for the compliance matrix from Appendix A to obtain linearized approximations for the anisotropic parameters defined in Appendix B. We assume that the weaknesses of both fracture systems are small ($\Delta_{Ni} \ll 1$ and $\Delta_{Ti} \ll 1$) so that the anisotropy of the effective monoclinic medium is weak. Keeping only terms linear in Δ_{Ni} and Δ_{Ti} leads to the expressions listed below. The parameter $\delta^{(3)}$ is not given here since it has no influence on the NMO velocities of horizontal events.

$$V_{P0} = V_P\left[1 - \frac{(1-2g)^2}{2}(\Delta_{N1} + \Delta_{N2})\right]. \quad \text{(C-1)}$$

$$V_{S0} = V_S\left[1 - \frac{\Delta_{T1}}{4}(1+\cos 2\phi_1) - \frac{\Delta_{T2}}{4}(1+\cos 2\phi_2)\right]. \quad \text{(C-2)}$$

$$\epsilon^{(1)} = -2g\{[(1-g)\Delta_{N1} + (\Delta_{T1} - g\Delta_{N1})\cos^2\phi_1]\sin^2\phi_1 + [(1-g)\Delta_{N2} + (\Delta_{T2} - g\Delta_{N2})\cos^2\phi_2]\sin^2\phi_2\}. \quad \text{(C-3)}$$

$$\epsilon^{(2)} = -2g\{[(1-g)\Delta_{N1} + (\Delta_{T1} - g\Delta_{N1})\sin^2\phi_1]\cos^2\phi_1 + [(1-g)\Delta_{N2} + (\Delta_{T2} - g\Delta_{N2})\sin^2\phi_2]\cos^2\phi_2\}. \quad \text{(C-4)}$$

$$\delta^{(1)} = -2g\{[(1-2g)\Delta_{N1} + \Delta_{T1}]\sin^2\phi_1 + [(1-2g)\Delta_{N2} + \Delta_{T2}]\sin^2\phi_2\}. \quad \text{(C-5)}$$

$$\delta^{(2)} = -2g\{[(1-2g)\Delta_{N1} + \Delta_{T1}]\cos^2\phi_1 + [(1-2g)\Delta_{N2} + \Delta_{T2}]\cos^2\phi_2\}. \quad \text{(C-6)}$$

$$\gamma^{(1)} = \left[2(\Delta_{T1} - g\Delta_{N1})\cos^2\phi_1 - \frac{\Delta_{T1}}{2}\right]\sin^2\phi_1 + \left[2(\Delta_{T2} - g\Delta_{N2})\cos^2\phi_2 - \frac{\Delta_{T2}}{2}\right]\sin^2\phi_2. \quad \text{(C-7)}$$

$$\gamma^{(2)} = \left[2(\Delta_{T1} - g\Delta_{N1})\sin^2\phi_1 - \frac{\Delta_{T1}}{2}\right]\cos^2\phi_1 + \left[2(\Delta_{T2} - g\Delta_{N2})\sin^2\phi_2 - \frac{\Delta_{T2}}{2}\right]\cos^2\phi_2. \quad \text{(C-8)}$$

$$\zeta^{(1)} = \frac{g}{4}[2g(\Delta_{N1}\sin 2\phi_1 + \Delta_{N2}\sin 2\phi_2) - (\Delta_{T1} - g\Delta_{N1})\sin 4\phi_1 - (\Delta_{T2} - g\Delta_{N2})\sin 4\phi_2]. \quad \text{(C-9)}$$

$$\zeta^{(2)} = \frac{g}{4}[2g(\Delta_{N1}\sin 2\phi_1 + \Delta_{N2}\sin 2\phi_2) + (\Delta_{T1} - g\Delta_{N1})\sin 4\phi_1 + (\Delta_{T2} - g\Delta_{N2})\sin 4\phi_2]. \quad \text{(C-10)}$$

$$\zeta^{(3)} = g(1-2g)(\Delta_{N1}\sin 2\phi_1 + \Delta_{N2}\sin 2\phi_2). \quad \text{(C-11)}$$

The values V_P and V_S are the P- and S-wave velocities in the isotropic background, and

$$g \equiv \frac{V_S^2}{V_P^2}. \quad \text{(C-12)}$$

Since the parameters of the effective monoclinic model depend on only eight parameters of the fractures and background medium, not all of the anisotropic coefficients are independent. Combining equations (C-9)–(C-11) yields

$$\frac{\zeta^{(3)}}{\zeta^{(1)} + \zeta^{(2)}} = \frac{1}{g} - 2. \quad \text{(C-13)}$$

It can be proved that this result remains valid for any strength of the anisotropy. Another relation between the effective coefficients, which follows from equations (C-3)–(C-8), has the form

$$\delta^{(1)} - \delta^{(2)} = 4g\left(\gamma^{(1)} - \gamma^{(2)}\right) + \frac{1-2g}{1-g}\left(\epsilon^{(1)} - \epsilon^{(2)}\right). \quad \text{(C-14)}$$

Equation (C-14) coincides with the constraint derived in part II for the effective orthorhombic medium caused by one system of fractures in a VTI background.

APPENDIX D

ESTIMATION OF FRACTURE PARAMETERS IN THE WEAK-ANISOTROPY LIMIT

The linearized approximations from Appendix C can be used to invert the anisotropic parameters of monoclinic media for the orientation and compliances of both fracture sets. A convenient way of performing this inversion procedure is outlined here.

Three ζ-coefficients combined in the form [equation (C-13)]

$$\frac{\zeta^{(3)}}{\zeta^{(1)} + \zeta^{(2)}} = \frac{1}{g} - 2 \quad \text{(D-1)}$$

give an estimate of g or the V_S/V_P ratio [see equation (C-12)] in the background. To avoid errors stemming from dividing two small numbers, g can be approximately found from the ratio of vertical velocities: $g \approx V_{S0}^2/V_{P0}^2$ [see equations (C-1) and (C-2)].

Two combinations,

$$\delta^{(1)} + \delta^{(2)} = -2g[(1-2g)(\Delta_{N1} + \Delta_{N2}) + (\Delta_{T1} + \Delta_{T2})] \quad \text{(D-2)}$$

and

$$\epsilon^{(1)} + \epsilon^{(2)} + g(\gamma^{(1)} + \gamma^{(2)}) = -\frac{g}{2}[4(1-g)(\Delta_{N1} + \Delta_{N2}) + (\Delta_{T1} + \Delta_{T2})], \quad \text{(D-3)}$$

can be used to find the sums of the normal and tangential compliances:

$$\Delta_{N1} + \Delta_{N2} = \frac{A - B}{3 - 2g} \equiv \mathcal{S}_{\Delta_N} \quad \text{(D-4)}$$

and

$$\Delta_{T1} + \Delta_{T2} = \frac{4(g-1)A + (1-2g)B}{3-2g} \equiv \mathcal{S}_{\Delta_T}, \quad \text{(D-5)}$$

where

$$A = \frac{\delta^{(1)} + \delta^{(2)}}{2g} \quad \text{and} \quad B = \frac{2}{g}\left[\epsilon^{(1)} + \epsilon^{(2)} + g\left(\gamma^{(1)} + \gamma^{(2)}\right)\right].$$

Equations (C-7) and (C-8) can be rewritten in the form

$$\Delta_{T1}\cos 2\phi_1 + \Delta_{T2}\cos 2\phi_2 = 2\left(\gamma^{(1)} - \gamma^{(2)}\right) \equiv \mathcal{D}_\gamma. \quad \text{(D-6)}$$

Combined with the linearized equation (9),

$$\Delta_{T1}\sin 2\phi_1 + \Delta_{T2}\sin 2\phi_2 = 0, \quad \text{(D-7)}$$

equation (D-6) can be solved for Δ_{T1} and Δ_{T2}:

$$\Delta_{T1} = \frac{\mathcal{D}_\gamma \sin 2\phi_2}{\sin 2(\phi_2 - \phi_1)}, \quad \Delta_{T2} = \frac{-\mathcal{D}_\gamma \sin 2\phi_1}{\sin 2(\phi_2 - \phi_1)}. \quad \text{(D-8)}$$

Substituting equation (D-8) into equation (D-5) yields a relationship between the fracture azimuths:

$$\mathcal{D}_\gamma \cos(\phi_2 + \phi_1) = \mathcal{S}_{\Delta_T}\cos(\phi_2 - \phi_1). \quad \text{(D-9)}$$

Note that the denominator in equations (D-8) does not vanish for $\Delta_{T1} = \Delta_{T2}$ because the azimuths ϕ_1 and ϕ_2 in this case have opposite signs ($\phi_1 = -\phi_2$).

Similarly, equations (C-3), (C-4), (C-9), and (C-10) can be combined to obtain

$$\Delta_{N1}\cos 2\phi_1 + \Delta_{N2}\cos 2\phi_2 = \frac{\epsilon^{(1)} - \epsilon^{(2)}}{2g(1-g)} \equiv \mathcal{D}_\epsilon \quad \text{(D-10)}$$

and

$$\Delta_{N1}\sin 2\phi_1 + \Delta_{N2}\sin 2\phi_2 = \frac{\zeta^{(2)} + \zeta^{(1)}}{g^2} \equiv \mathcal{S}_\zeta. \quad \text{(D-11)}$$

Equations (D-10) and (D-11) give the following expressions for the normal weaknesses:

$$\Delta_{N1} = \frac{\mathcal{D}_\epsilon \sin 2\phi_2 - \mathcal{S}_\zeta \cos 2\phi_2}{\sin 2(\phi_2 - \phi_1)}, \qquad \Delta_{N2} = \frac{-\mathcal{D}_\epsilon \sin 2\phi_1 + \mathcal{S}_\zeta \cos 2\phi_1}{\sin 2(\phi_2 - \phi_1)}. \quad \text{(D-12)}$$

Substituting equation (D-12) into equation (D-4), we find a second relation between the azimuths:

$$\mathcal{D}_\epsilon \cos(\phi_2 + \phi_1) + \mathcal{S}_\zeta \sin(\phi_2 + \phi_1) = \mathcal{S}_{\Delta_N}\cos(\phi_2 - \phi_1). \quad \text{(D-13)}$$

Equations (D-9) and (D-13) can be solved for $\phi_2 + \phi_1$ and $\phi_2 - \phi_1$:

$$\phi_2 + \phi_1 = \tan^{-1}\left[\frac{\mathcal{D}_\gamma \mathcal{S}_{\Delta_N} - \mathcal{D}_\epsilon \mathcal{S}_{\Delta_T}}{\mathcal{S}_{\Delta_T}\mathcal{S}_\zeta}\right]. \quad \text{(D-14)}$$

Using equation (D-9), we find

$$\phi_2 - \phi_1 = \cos^{-1}\left[\frac{\mathcal{D}_\gamma}{\mathcal{S}_{\Delta_T}}\cos(\phi_2 + \phi_1)\right]. \quad \text{(D-15)}$$

Equations (D-14) and (D-15) make it possible to determine the fracture azimuths ϕ_1 and ϕ_1.

After recovering the fracture orientation, we can compute the four weaknesses Δ_{Ti} and Δ_{Ni} from equations (D-8) and (D-12). Finally, equations (C-1) and (C-2) yield the P- and S-wave velocities in the background.

APPENDIX E

SPECIAL CASE OF EQUAL TANGENTIAL WEAKNESSES

Suppose the tangential weaknesses of the crack systems are equal, so that

$$\Delta_{T1} = \Delta_{T2} \equiv \Delta_T. \quad \text{(E-1)}$$

Then it follows from equation (9) that

$$\phi_1 = -\phi_2 \equiv \phi. \quad \text{(E-2)}$$

Substituting equations (E-1) and (E-2) into the weak-anisotropy approximations (C-1)–(C-11) yields

$$V_{P0} = V_P\left[1 - \frac{(1-2g)^2}{2}(\Delta_{N1} + \Delta_{N2})\right], \quad \text{(E-3)}$$

$$V_{S0} = V_S\left[1 - \frac{\Delta_T}{2}(1 + \cos 2\phi)\right], \quad \text{(E-4)}$$

$$\epsilon^{(1)} = -2g\left\{(1-g)(\Delta_{N1} + \Delta_{N2}) + [2\Delta_T - g(\Delta_{N1} + \Delta_{N2})]\cos^2\phi\right\}\sin^2\phi, \quad \text{(E-5)}$$

$$\epsilon^{(2)} = -2g\left\{(1-g)(\Delta_{N1} + \Delta_{N2}) + [2\Delta_T - g(\Delta_{N1} + \Delta_{N2})]\sin^2\phi\right\}\cos^2\phi, \quad \text{(E-6)}$$

$$\delta^{(1)} = -2g\{(1-2g)(\Delta_{N1} + \Delta_{N2}) + 2\Delta_T\}\sin^2\phi, \quad \text{(E-7)}$$

$$\delta^{(2)} = -2g\{(1-2g)(\Delta_{N1} + \Delta_{N2}) + 2\Delta_T\}\cos^2\phi, \quad \text{(E-8)}$$

$$\gamma^{(1)} = \left\{2[2\Delta_T - g(\Delta_{N1} + \Delta_{N2})]\cos^2\phi - \Delta_T\right\}\sin^2\phi, \quad \text{(E-9)}$$

$$\gamma^{(2)} = \left\{2[2\Delta_T - g(\Delta_{N1} + \Delta_{N2})]\sin^2\phi - \Delta_T\right\}\cos^2\phi, \quad \text{(E-10)}$$

$$\zeta^{(1)} = 2g^2(\Delta_{N1} - \Delta_{N2})\sin\phi\cos^3\phi, \quad \text{(E-11)}$$

$$\zeta^{(2)} = 2g^2(\Delta_{N1} - \Delta_{N2})\sin^3\phi\cos\phi, \quad \text{(E-12)}$$

and

$$\zeta^{(3)} = g(1-2g)(\Delta_{N1} - \Delta_{N2})\sin 2\phi. \quad \text{(E-13)}$$

Equations (E-3)–(E-13) are much easier to invert for the fracture parameters than the more general expressions of Appendix C. Having estimated g from either equation (D-1) or the V_{S0}/V_{P0} ratio, we obtain the fracture azimuth as

$$\frac{\delta^{(1)}}{\delta^{(2)}} = \frac{\zeta^{(2)}}{\zeta^{(1)}} = \tan^2\phi. \quad \text{(E-14)}$$

Note that the angle between the two systems of cracks is equal to 2ϕ. The tangential weakness Δ_T can be found from the shear-wave splitting coefficient $\gamma^{(S)}$ which, in the limit of weak

anisotropy, reduces to the difference between $\gamma^{(2)}$ and $\gamma^{(1)}$:

$$\gamma^{(S)} = \gamma^{(2)} - \gamma^{(1)} = -\Delta_T \cos 2\phi. \qquad \text{(E-15)}$$

Then any of equations (E-11)–(E-13) for the ζ coefficients give the difference between the normal weaknesses $\Delta_{N1} - \Delta_{N2}$. The sum $\Delta_{N1} + \Delta_{N2}$ can be determined, for instance, from $\delta^{(1)}$ and $\delta^{(2)}$ [equations (E-7) and (E-8)]:

$$\Delta_{N1} + \Delta_{N2} = \frac{1}{2g-1}\left(\frac{\delta^{(1)} + \delta^{(2)}}{2g} + 2\Delta_T\right). \qquad \text{(E-16)}$$

Combined with the difference $\Delta_{N1} - \Delta_{N2}$ obtained earlier, equation (E-16) yields the individual values of the normal weaknesses Δ_{N1} and Δ_{N2}.